Computational optimization of transcranial focused ultrasound stimulation: Toward noninvasive, selective stimulation of deep brain structures

Cite as: Appl. Phys. Lett. **118**, 233702 (2021); https://doi.org/10.1063/5.0052743
Submitted: 01 April 2021 . Accepted: 27 May 2021 . Published Online: 10 June 2021

A. De Angelis, M. Leonetti, F. Apollonio, M. Liberti, S. M. Aglioti, and G. Ruocco

Applied Physics Letters ARTICLE scitation.org/journal/apl

Computational optimization of transcranial focused ultrasound stimulation: Toward noninvasive, selective stimulation of deep brain structures

Cite as: Appl. Phys. Lett. **118**, 233702 (2021); doi: 10.1063/5.0052743
Submitted: 1 April 2021 · Accepted: 27 May 2021 ·
Published Online: 10 June 2021

A. De Angelis,[1,a)] M. Leonetti,[1,2] F. Apollonio,[1,3] M. Liberti,[1,3] S. M. Aglioti,[1,4] and G. Ruocco[1,5]

AFFILIATIONS

[1]Center for Life Nano- and Neuro-Science, Istituto Italiano di Tecnologia, Rome 00161, Italy
[2]CNR NANOTEC-Institute of Nanotechnology, Soft and Living Matter Lab, Rome 00185, Italy
[3]Department of Information Engineering, Electronics and Telecommunications, Sapienza University of Rome, 00184, Italy
[4]Fondazione Santa Lucia, IRCCS, Rome 00179, Italy
[5]Department of Physics, Sapienza University of Rome, 00185, Italy

[a)]**Author to whom correspondence should be addressed:** annalisa.deangelis@iit.it

ABSTRACT

Low-intensity focused ultrasound is emerging as a high-resolution highly selective alternative to standard noninvasive transcranial brain stimulation techniques. A major challenge in using ultrasound devices is designing a stimulator capable of efficiently focusing the acoustic wave to selectively target a specific brain region by compensating for the wavefront distortions induced by the intact skull. Single-element transducers are efficient in stimulating cortical areas in both non-human and human primates. However, reaching deeper brain structures with millimeter resolution and high specificity requires the use of *ad hoc* multi-element devices characterized by a specific number of piezoelectric elements that optimize the energy deposition in the focal region while simultaneously minimizing the off-focus dispersion. The high cost and complexity of adequately controlling the thousands of elements used generally for such stimulators have limited their use in neuromodulation applications. This study defines the optimal configuration of a multi-element stimulator for low-intensity focused ultrasound through a full-wave realistic numerical model that includes both the stimulator geometry and a detailed anatomical head model. The performance of the device was evaluated. We investigated the influence of the number of piezoelectric elements in the stimulator on its transcranial focusing capabilities. Our results confirm that the focusing optimization improves as the number of elements increased (from 16 to 256). With only 96 point-sources, there was a good trade-off between cost and focusing efficiency. Our study provides a cost-effective stimulator design that enables a standard focusing procedure and a steering technique enacted without prior knowledge about the skull's local acoustic impedance.

Focused ultrasound stimulation (FUS) is an emerging, noninvasive, focal, and ultra-selective technique for brain stimulation and modulation. Neurosurgical applications indicate that the ablative use of high-intensity ultrasound can help to treat patients with movement disorders[1] like Parkinson's disease,[2] brain tumors,[3] and neuropathic pain.[4] Recently, the use of low-intensity FUS (0.5–100 W/cm^2, corresponding to a pressure range of 0.1–1 MPa) proved effective in modulating neuronal activity in both non-human[5–8] and human primates.[9–13] Thus, it is emerging as a highly specific and high-resolution alternative to the commonly used noninvasive brain stimulation and modulation techniques (like transcranial magnetic or electric stimulation).[14] A major challenge in designing a stimulator is in delivering the acoustic wave so that it selectively targets a specific brain region, despite the reflections from and scattering by the skull.[15] Indeed, the strong acoustic impedance mismatches at the skin/bone and bone/dura mater interfaces as well as the heterogeneous bone structure (the lateral tables are dense, whereas the central diploe is porous), resulted in a severe loss of acoustic energy, distortion of the propagating beam, and a consequent ill-definition of the focus. The overall effect is a degradation of the stimulation performance.

Phased-array technology promises to improve the focusing performance. Instead of using a single-element stimulator, several smaller

transducers, assembled on a flat or spherical casing, can be individually driven in phase and amplitude to tailor the wavefront of the propagating acoustic beam.[16–18] Expensive, large, and fully populated arrays have been designed for targeted thermal ablation,[2–4,19,20] as less acoustic power is deposited on the scalp and there are more degrees of freedom for off-axis steering and multi-targeting.

Conversely, cheaper solutions, with lower intensities, could be used for noninvasive neuromodulation or stimulation applications. The only example in the literature is the work of Chaplin *et al.*,[21] who tested a FUS stimulator composed of 128 randomized circular elements distributed on a spherical cap. It was specifically designed for the highly selective stimulation of the sensorimotor cortex in macaques. However, these authors characterized their device only through free water simulations and did not investigate the effectiveness of making the aberration corrections required for realistic contexts. Thus, improving the transcranial transmission and deep brain focalization of the ultrasound beam needs more accurate, simulation-based investigations to determine the impact of the device parameters on its performance and, ultimately, to help the design process.[15,18,22,23]

Here, we provide an optimization procedure for designing the focusing and steering capabilities of a stimulator. It employs a detailed numerical model of the actual geometry of the stimulator and highly realistic detailed models reproducing the anatomical complexity of the human head (Fig. 1). Specifically, we study the impact of the number of piezoelectric elements on the stimulation efficiency in deep regions of the human brain. The simulation, including the models of the ultrasound stimulator and the human head, was implemented in the simulation software Sim4Life.[24] The stimulator model was built directly in Sim4Life via a Python script. It consisted of a spherical cap with an aperture (D) of 150 mm and a radius of curvature (corresponding to the focal depth F) of 120 mm (focal ratio, $F/D = 0.8$). D and F were chosen so that the stimulator geometry matched that of the human head and to keep the focal ratio between 0.5 and 1, which gives a better focal gain and spatial resolution.[21] The internal surface of the spherical cap, modeled as a reflecting material, accommodated a number of randomized circular piezoelectric elements [an example is shown in Fig. 1(c)]. The random positioning of the elements reduces the unwanted grating lobes compared to a uniform configuration.[21,25] The sparsity allowed a large aperture for steering the wide beam without needing an excessive number of elements.[26,27] The element diameter was 6 mm (as having smaller elements would increase the electrical impedance of the electrodes and decrease the piezoelectric conversion efficiency[21]). Six configurations with different numbers of elements were tested (16, 32, 64, 96, 128, and 256). The percentage of the total active area was different in each case.

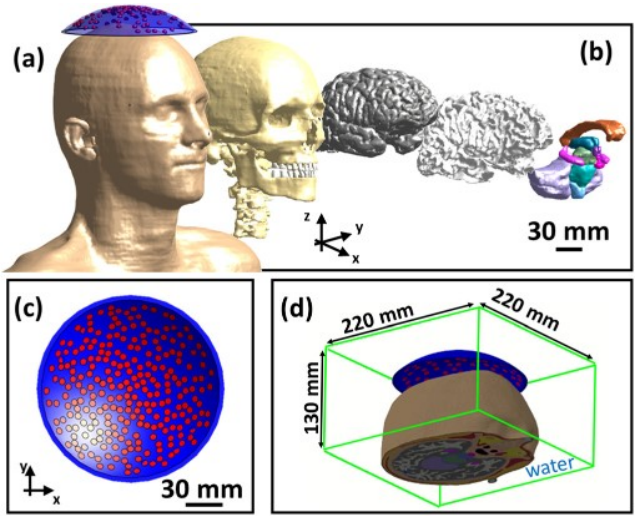

FIG. 1. (a) Multi-source stimulator positioned above the head. (b) Main structures in the head models (from left to right: cortical and cancellous bone, gray, and white matter, deep structures including the corpus callosum, thalamus, hypothalamus, hypophysis, hippocampus, midbrain, pons, medulla oblongata, and cerebellum). (c) Enlargement of the multi-source stimulator showing the randomly distributed circular elements. (d) Simulated domain including the stimulator, the head truncated 10 mm below the geometrical focus, and the green bounding box representing the water background.

The human head models used in our study were derived from Duke [Figs. 1(a) and 1(b)], a 34-year-old male full-body model from the Virtual Population database,[28] and MIDA,[29] a model of the head of a 29-year-old female. Both head models have 38 individual tissues (Fig. S1) and 11 brain structures [Fig. 1(b)].

The propagation of an acoustic wave through the heterogeneous regions in the head was simulated in a 3D full-wave acoustic solver in Sim4Life, which encompassed all the relevant phenomena (reflections due to variations and discontinuities of the acoustic impedance, standing waves, and the combined effect of absorption and scattering). Specific properties, such as the speed of sound, mass density, and attenuation coefficient, were automatically assigned to each material from a parameter library in Sim4Life. These parameters were set after a comprehensive scientific literature review.[30] The solver was based on the Westervelt–Lighthill equation,[31] extended with a density variation term that accounts for the large differences in the acoustic impedances of the heterogeneous tissues, mainly in the skull layers, resulting in the linear acoustic pressure wave equation,

$$\rho \nabla \frac{1}{\rho} \nabla p - \frac{1}{c^2} \frac{\partial^2 p}{\partial t^2} - \frac{a}{c^2} \frac{\partial p}{\partial t} = 0, \tag{1}$$

where p is the acoustic pressure, ρ and c denote the mass density and the speed of sound of the material, respectively, and t is the time. The parameter a describes the absorption behavior of the head structures,

$$a = 2\alpha \sqrt{\frac{\alpha^2 c^4}{\omega^2} + c^2}, \tag{2}$$

where α is the attenuation coefficient and ω is the angular frequency of the pressure wave. In our simulations, we used the linear Eq. (1) as it has been shown[32] that the nonlinear contribution is negligible for the low acoustic pressures used here ($\leq$0.4 MPa; see Table I). Moreover, only longitudinal waves were considered, as the incident angle of the acoustic beam to the skull surface is close to orthogonal due to the chosen geometry and the horizontal positioning of the stimulator above the head [Fig. 1(a)]. Because of this, the conversion mode of the propagating waves in the shear waves should not be significant.[15,33] Each element of the stimulator was modeled as a source of a sinusoidal acoustic wave with an amplitude that depends on the active area of each stimulator (Table I), providing a constant total power of 30 W and a fundamental frequency of 500 kHz.[15,34,35]

TABLE I. Pressure generated from each active element of the six stimulator configurations and the corresponding active area.

Number of elements	Applied pressure (MPa)	Active area (%)
16	0.4	2.5
32	0.3	5
64	0.2	10
96	0.18	15
128	0.16	20
256	0.1	40

The partial difference Eq. (1) was solved in a 3D domain using the finite difference in the time domain (FDTD) method. The computational domain [a bounding box of $220 \times 220 \times 130\,\text{mm}^3$; Fig. 1(d)] was discretized into uniform cubic Cartesian cells with a spatial resolution of $\lambda/10$ (0.3 mm), so that there were over 200×10^6 voxels. The computational domain was terminated with perfectly matched layers to prevent reflections from the boundaries.[36] Altogether, 175 periods of the acoustic wave, corresponding to a propagation time of 350 μs at 500 kHz, were chosen to achieve the steady state, as longer durations resulted in less than a 0.1% difference in terms of absolute pressure. A complete description of the simulation environment and a validation of the ultrasound propagation solver are reported in Neufeld *et al.*[37] The simulations were run on a PC with an Intel® Core™ i7-9800X CPU at 3.80 GHz, with 64 GB of RAM and an NVIDIA GeForce RTX 2070 GPU.

We first investigated the focusing performance of the stimulator with different numbers of sources before and after simulation-based optimization using the Duke model. The ultrasound focus was optimized by placing a virtual source at the targeted brain region and recording the pressure waves at the coordinates of the array elements in the helmet. Then the recorded signal was phase conjugated and applied at each array element so that the focus was at the target.[38–40]

This numerical approach could represent a promising and potentially patient-specific alternative (if the simulations are informed by imaging like magnetic resonance or computer tomography) to purely analytical or complex and time-consuming experimental focusing, such as employing an implanted hydrophone in which the wavefront phase correction is inferred directly by measuring the acoustic pressure at the target or indirectly by magnetic-resonance acoustic-radiation-force imaging.[18] In Figs. 2(a)–2(h), the distribution of the acoustic intensity (defined as $p^2/2\rho c$) in the longitudinal plane (yz) of the head before [Figs. 2(a)–2(d)] and after [Figs. 2(e)–2(h)] the correction of the beam aberrations is shown for the stimulators with 64, 96, 128, and 256 elements.

The size and shape of the focal spot in the transcranial propagation were affected by the skull, resulting in the formation of axial and lateral lobes and secondary hot spots. After the optimization [Figs. 2(e)–2(h)], we retrieved a transversal FWHM and a longitudinal FWHM of 1.8 and 8 mm, respectively, for all the stimulators investigated (which is the same as the focal volume obtained in free water; Fig. S2). Indeed, the number of elements in each helmet did not affect the focus size but did influence the focus quality. The axial and lateral lobes decreased as the number of elements increased and disappeared when 256 elements were simulated. Moreover, the ratio of the peak intensity of the residual lobes to that at the focus was lower than 0.1 (−10 dB) for 96, 128, and 256 elements.

In Fig. 2(i), the focusing effectiveness (FE), evaluated as the ratio between the peak intensity at the focus and the power from the stimulators (input power 30 W), shows that the natural focusing capability of the stimulator and its optimized capability both improved with a larger number of elements. In the optimized case (red squares), the FE reached the expected values considering the different percentages of the active area of each stimulator (Table I). Figure 2(i) shows that the stimulators with 16 and 32 elements had a very low FE in both the unoptimized and optimized cases.

We also investigated the volumetric focality of the stimulator. The focality was optimized by maximizing the focal pressure levels while simultaneously minimizing the pressure outside the focal volume. Figure 3(a) shows binary maps (above and below a threshold) of the predicted pressure field in the coronal focal slice of the brain. The areas where the acoustic pressure exceeds the threshold (shown at the top of the panels) are white, whereas the under-threshold regions are black (only a few representative thresholds are shown). Each row shows the pressure maps induced in the brain by a different number of sources.

Figure 3(b) shows the number of voxels producing different acoustic pressures in the whole brain volume (the volume of a voxel was 0.027 m). As expected, the 16-element stimulator was not able to

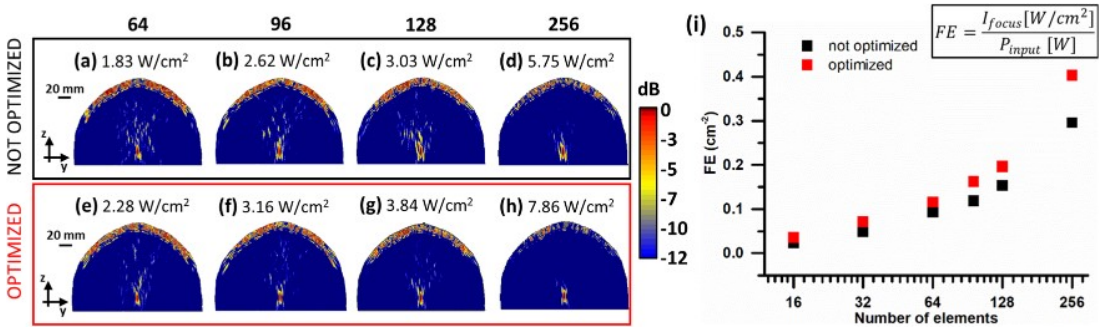

FIG. 2. Focal plane (yz) head slices. (a)–(h) Acoustic intensity maps for 64, 96, 128, and 256 elements before (a)–(d) and after (e)–(h) phase correction. The acoustic intensity in each map is the corresponding average peak intensity at the geometrical focus. (i) The focusing effectiveness (FE) plotted against the number of elements. FE is defined as the ratio of the intensity induced at the focus and the input power from the stimulator. Black and red squares are non-optimized and optimized cases, respectively.

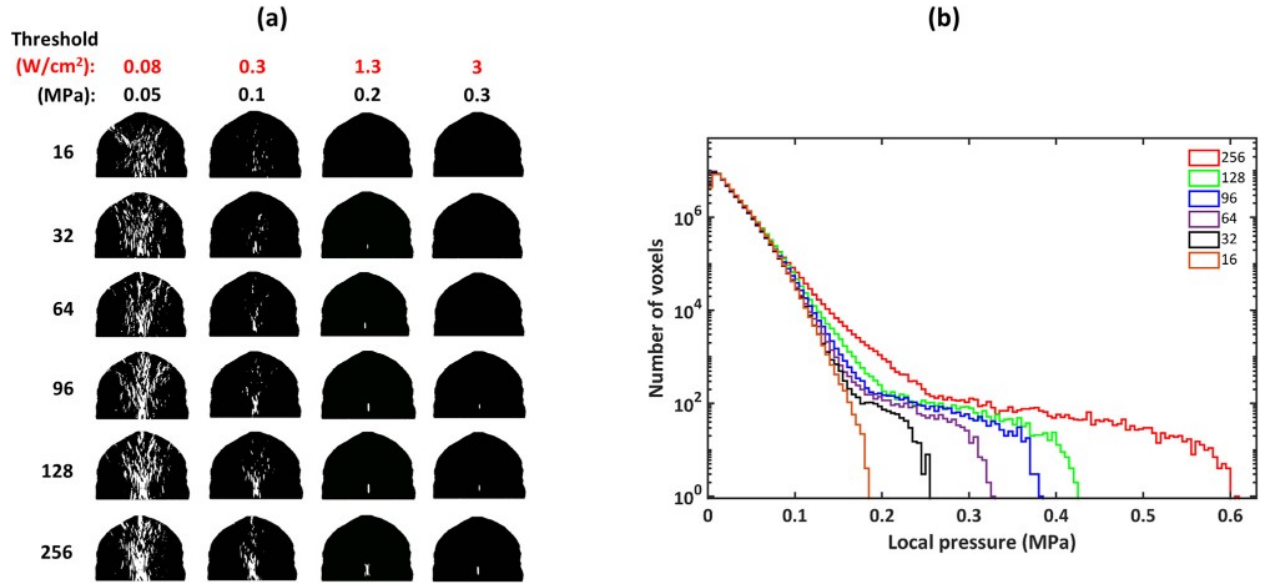

FIG. 3. (a) Binary maps of brain slices through the coronal plane. Highlighted in white are above-threshold areas. Below-threshold areas are black. (b) Spatial distribution of the induced pressure on the simulated brain volume (volume of a voxel was 0.027 mm^3 and the bin width was 0.005 MPa).

focalize the acoustic pressure efficiently [first row of Fig. 3(a)] and reached a maximum of only 0.17 MPa [Fig. 3(b)]. A local pressure of between 0.1 and 0.2 MPa was induced in the other cases due to the focalization. Only the stimulators with the highest numbers of elements (96, 128, and 256) were able to focalize a pressure >0.3 MPa, which they realized over a broader range of pressure values, as indicated by the plateau in the distributions associated with these stimulators [Fig. 3(b)].

Our results confirm that for a stimulator with a constant focal ratio, using at least 96 elements that cover the full aperture results in good performance. Among them, even though the 256-element stimulator was undoubtedly the most efficient, the 96-element device had a more than satisfactory performance, and thus, it is a cost-effective alternative.

The stimulator was next tested on the MIDA model to confirm the robustness of the focusing efficiency. Despite the well-known anatomical differences between males and females, our focusing optimization led to very similar results (Fig. S3), confirmed by the spatial distribution of the pressure in Fig. S4. This is due to the ability of this technique to adapt the focusing for the specific anatomical details of each head.

Moreover, to assess the effectiveness of the multi-targeting and steering of the stimulator, we first optimized the focus for a second target 12 mm from the previous one in the Duke model. We steered the focal point by linearly changing the phase of the different sources. The phase delay Φ_i for each stimulator was calculated according to the following simple constant phase gradient formula:

$$\Phi_i = \varphi_i + \left(\left|d_{focus}\right| - \left|d_{target}\right|\right)\frac{2\pi}{\lambda},$$

where φ_i is the original phase delay and $\left|d_{focus}\right|$ and $\left|d_{target}\right|$ are the distances of the center of each element from the original focal point and the new target point, respectively.

Unlike phase conjugation, the technique proposed for steering does not require any knowledge of the acoustic impedance between each source (array element) and the target. This approach avoids the need for expensive and time-consuming experimental measurements in addition to the simulations required by the previous focusing optimization approach. The analytic steering technique is efficient if the sources are close to the scalp. It is a faster alternative to scanning the ultrasound focus over small volumes of the region of interest in the brain.

Figure 4(a) shows the optimized refocusing of the beam at the desired location in the focal plane (no shift) and after the beam was steered (with shifts of 2, 4, and 6 mm along the *x*-, *y*-, and *z*-axes) for a 96-element stimulator. It is possible to electronically steer the beam off-axis by at least 12 mm while maintaining the peak pressure higher than 50% of the peak pressure at the geometrical focus (0.38 MPa), as shown in Fig. 4(b). Three different random configurations of the 96 elements were investigated (Fig. S5) to verify that the predicted results were independent of the specific positioning. The average targeting and steering accuracy were of the order of the voxel resolution (0.3 mm) for the *x*- and *y*-axes and below 1 mm for the *z*-axis. Figures 4(b)–4(d) show the means and standard deviations of (b) the focal peak pressure, (c) the FWHM focal volume, and (d) the spread-to-focalized volume ratio for the simulated steering of the beams with the three random configurations. The focus degraded when steered. Nevertheless, the FWHM focal volume for a shift of 6 mm was still comparable to the expected volume of about 15 mm^3 [Fig. 4(c)]. More interestingly, the ratio of the FWHM volume outside the focus to that at the focus was between 0 and 0.06 [Fig. 4(d)].

Other areas at different Euclidean distances from the geometrical focus were also targeted [i.e., the midbrain, thalamus, amygdala, and insula; Fig. S6(a)], showing the ability to move the acoustic focus precisely onto specific targets within a volume of about 70 cm^3 in the deep brain. The focusing quality decreased when the focus was moved

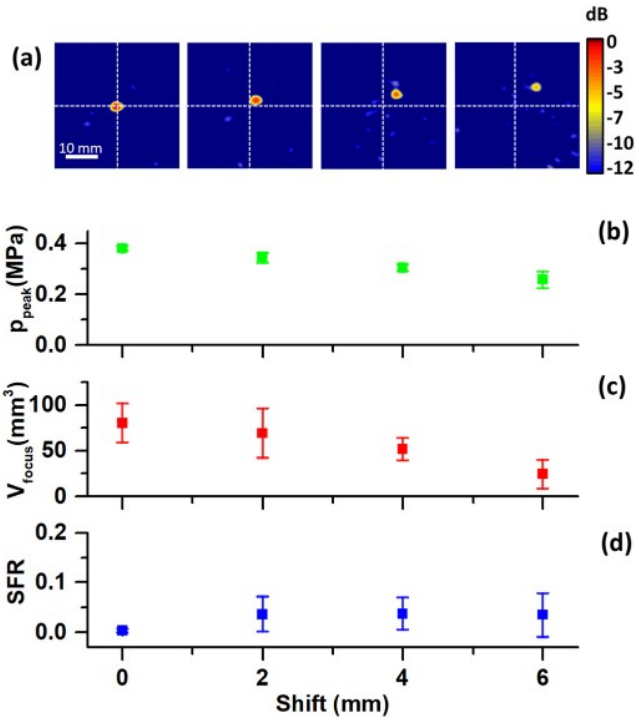

FIG. 4. (a) Enlarged pressure maps for the transversal focal plane (*xy*) when the acoustic beam was electronically refocused on a different target (e.g., the thalamus) and electronically steered with increments of 2 mm along the *x*, *y*, and *z*-axes. The impact of the steering on (b) the peak pressure, (c) the FWHM focal volume, and (d) the spread-to-focalized volume ratio (SFR), reported in terms of the mean and standard deviation for three different randomizations of the 96 elements.

from deeper areas [Figs. S6(b) and S6(c)] to more peripheral ones [Figs. S6(d) and S6(e)]. Modulating the pressure amplitude from each channel based on the specific transmission (or absorption) by the bone segment crossed by the acoustic wave should further improve our focusing and steering strategy.

In summary, we investigated the performance of an FUS device with different numbers of piezoelectric elements optimized by phase conjugation. We adopted a numerical model to represent the real neurostimulation scenario, including both the stimulator geometry and a detailed anatomical head model. The results show that the focusing can be optimized with at least 96 piezoelectric elements. The beam can be focused and steered to stimulate specific functional areas without mechanical repositioning. Thus, a 96-element stimulator likely represents a good trade-off between cost, focusing, and pressure levels induced in the brain volume.

Low-intensity FUS is gaining momentum and promises to become highly relevant for clinical application in the near future.[41] Our simulation study paves the way for the construction of an improved generation of devices with the unprecedented property of stimulating noninvasively deep regions of the brain without affecting the superficial regions. While such a device will require extensive testing in animal models, it has the potential to change the noninvasive brain stimulation radically, not only in healthy people but also for people with a variety of neuropsychiatric disorders.

See the supplementary material includes the acoustic pressure maps of free water propagation for all the investigated stimulators and the optimized focusing performance of the 96-element stimulator for a male and a female head model.

AUTHORS' CONTRIBUTIONS

All authors contributed equally to this work.

This study was funded by IIT Brain Magnet Program awarded to Salvatore M. Aglioti and the Italian Ministry of Health Grant (No. RF-2019-12368598) to Salvatore M. Aglioti and Giancarlo Ruocco.

DATA AVAILABILITY

The data that support the findings of this study are available from the corresponding author upon reasonable request.

REFERENCES

[1]N. Lipsman, M. L. Schwartz, Y. Huang *et al.*, Lancet Neurol. **12**, 462 (2013).
[2]W. J. Elias, D. Huss, T. Voss *et al.*, N. Engl. J. Med. **369**, 640 (2013).
[3]N. McDannold, G. T. Clement, P. Black *et al.*, Neurosurgery **66**, 323 (2010).
[4]E. Martin, D. Jeanmonod, A. Morel *et al.*, Ann. Neurol. **66**, 858 (2009).
[5]Y. Tufail, A. Matyushov, N. Baldwin *et al.*, Neuron **66**, 681 (2010).
[6]S. S. Yoo, A. Bystritsky, J. H. Lee *et al.*, Neuroimage **56**, 1267 (2011).
[7]T. Deffieux, Y. Younan, N. Wattiez *et al.*, Curr. Biol. **23**, 2430 (2013).
[8]J. Zou, L. Meng, Z. Lin *et al.*, Science **23**, 101066 (2020).
[9]W. Lee, H. Kim, Y. Jung *et al.*, Sci. Rep. **5**, 34026 (2015).
[10]J. K. Mueller, W. Legon, and W. J. Tyler, arXiv 1 (2015).
[11]W. Legon, P. Bansal, R. Tyshynsky *et al.*, Sci. Rep. **8**, 10007 (2018).
[12]W. Legon, L. Ai, P. Bansal, and J. K. Mueller, Hum. Brain Mapp. **39**, 1995 (2018).
[13]K. Yu, C. Liu, X. Niu, and B. He, IEEE Trans. Biomed. Eng. **1**, 1923 (2020).
[14]A. Bystritsky, A. S. Korb, P. K. Douglas *et al.*, Brain Stimul. **4**, 125 (2011).
[15]F. J. Fry and J. E. Barger, J. Acoust. Soc. Am. **63**, 1576 (1978).
[16]E. S. Ebbini and C. A. Cain, Int. J. Hyperthermia **7**, 953 (1991).
[17]J. White, G. T. Clement, and K. Hynynen, IEEE Trans. Ultrason., Ferroelectr., Freq. Control **52**, 1518 (2005).
[18]A. Kyriakou, E. Neufeld, B. Werner *et al.*, Int. J. Hyperthemia **30**, 36 (2014).
[19]D. Coluccia, J. Fandino, L. Schwyzer *et al.*, J. Ther. Ultrasound **17**, 1 (2014).
[20]S. J. Monteith, R. Medel, N. F. Kassell *et al.*, J. Neurosurg. **118**, 319 (2013).
[21]V. Chaplin, M. A. Phipps, and C. F. Caskey, Phys. Med. Biol. **63**, 105016 (2018).
[22]H. Salahshoor, M. G. Shapiro, and M. Ortiz, Appl. Phys. Lett. **117**, 033702 (2020).
[23]C. Pasquinelli, H. Montanaro, H. J. Lee *et al.*, J. Neural Eng. **17**, 046010 (2020).
[24]See https://Zurichmedtech.Com/Sim4life for "Sim4Life Zurich Med Tech (2021)."
[25]D. N. Stephens, D. E. Kruse, S. Qin, and K. W. Ferrara, IEEE Trans. Ultrason., Ferroelectr., Freq. Control **58**, 1590 (2011).
[26]L. A. Frizzell, S. A. Goss, J. T. Kouzmanoff, and J. M. Yang, Proc. IEEE Ultrason. Symp. **2**, 1319 (1996).
[27]L. R. Gavrilovi, IEEE Trans. Ultrason., Ferroelectr., Freq. Control **47**, 125 (2000).
[28]M. C. Gosselin, E. Neufeld, H. Moser *et al.*, Phys. Med. Biol. **59**, 5287 (2014).
[29]M. I. Iacono, E. Neufeld, E. Akinnagbe *et al.*, PLoS One **10**, e0124126 (2015).
[30]P.A. Hasgall, F. Di Gennaro, C. Baumgartner *et al.*, IT'IS, Database Version 4.0, 2018.
[31]P. J. Westervelt, J. Acoust. Soc. Am. **35**, 535 (1963).
[32]T. Deffieux and E. Konofagou, IEEE Trans. Ultrason., Ferroelectr., Freq. Control **57**, 2637 (2010).
[33]P. J. White, G. T. Clement, and K. Hynynen, Ultrasound Med. Biol. **32**, 1085 (2006).
[34]F. J. Fry, Ultrasound Med. Biol. **3**, 183 (1977).

[35]P. P. Ye, J. R. Brown, and K. B. Pauly, Ultrasound Med. Biol. **42**, 1512 (2016).
[36]W. C. Chew, J. M. Jin, and E. Michielssen, Microwave Opt. Technol. Lett. **15**, 363 (1997).
[37]E. Neufeld, A. Kyriacou, W. Kainz, and N. Kuster, J. Verif., Valid. Uncertainty Quantif. **1**, 031006 (2016).
[38]M. Fink, IEEE Trans. Ultrason., Ferroelectr., Freq. Control **39**, 555 (1992).
[39]M. Fink, G. Montaldo, and M. Tanter, Annu. Rev. Biomed. Eng. **5**, 465 (2003).
[40]M. Fink, C. Prada, F. Wu, and D. Cassereau, in *Ultrasonics Symposium* (IEEE, 1989), Vol. 2 p. 681.
[41]R. Beisteiner and A. M. Lozano, Adv. Sci. **7**, 2002026 (2020).